15 Estimation of Attitude from a Single-Direction Sensor

Lionel Magnis and Nicolas Petit

CONTENTS

15.1 INTRODUCTION

Consider a reference vector $\mathbf{a} = (\mathbf{a}_1\ \mathbf{a}_2\ \mathbf{a}_3)^{\mathrm{T}}$ expressed in the inertial frame. Then, the expression $a = (a_1\, a_2\, a_3)^{\mathrm{T}}$ of $\mathbf{a}$ in the body frame at time t is

$$a(t) = R(t)^{\mathrm{T}}\mathbf{a} \tag{15.1}$$

where $R(t)$ is the attitude matrix. The variable $a(t)$ is called a *vector observation* or *vector measurement*. This is the variable produced by a *direction sensor* such as a magnetometer or a Sun sensor, among several possibilities.

It is well known that measurements from a single-direction sensor do not allow us to know $R(t)$ completely. Yet, as we will see, it may be enough to give a satisfactory estimate, given certain assumptions about the rotational motion.

In this chapter, we assume that $\mathbf{a}$ is known and we consider the problem of estimating the rotation from measurements of the form (Equation 15.1). The difficulty of this problem is mostly defined by the nature of the rotation, which may be about a single axis, defining a planar measurement signal, or it may vary slightly, or it may be very complex for an arbitrary rotation; the three cases are illustrated in Figure 15.1. Assuming that $\mathbf{a}$ is constant, then $a(t)$ has constant norm. Hence, it is reasonable to represent it on a sphere.

The scope of this chapter encompasses the first two cases. We present simple, easy-to-implement estimators, when *a priori* information is known about the rotational motion. In Section 15.2, we consider single-axis rotation parameterized by a single angle, and give a straightforward estimator for it. We then consider the case where the axis of rotation is not constant but moving slightly, and some *a priori* information about its motion is known. We treat the two cases employing an

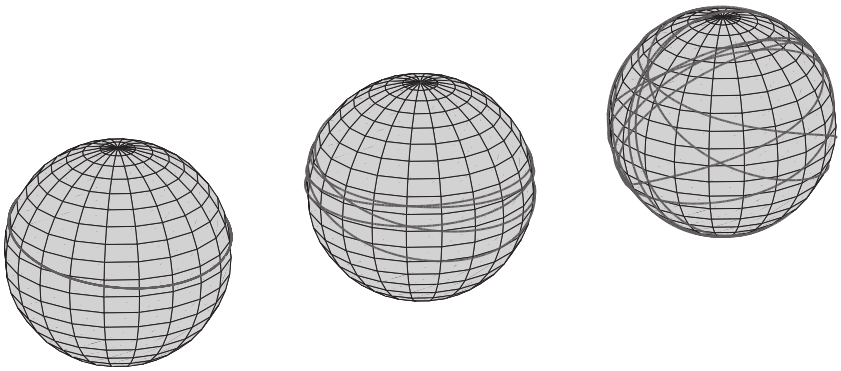

FIGURE 15.1 Measurement $a(t)$ for (left) single-axis rotation on a sphere, (middle) slightly varying, and (right) complex rotational motions.

Euler angle parametrization of the attitude. In Section 15.3, we consider a slow drift motion of the axis of rotation. An extension of the single-axis estimator is employed, which requires separate analyses of the phase and the modulus of a complex quantity. In Section 15.4, we consider a small-amplitude tilt of the axis of rotation. We propose a two-phase estimator obtained from careful decomposition of the signals based on natural frequency separation in the spectrogram of the measurement signals.

15.2 SINGLE-AXIS ROTATIONAL MOTION

We consider the case of single-axis (or *planar*) rotations. Such rotations correspond to a matrix $R(t)$ of constant axis, which can be written as

$$R(t) = r_{\mathbf{u}}(\psi(t)) \triangleq \cos\psi(t) I + \sin\psi(t)[\mathbf{u}_\times] + (1-\cos\psi(t))\mathbf{u}\mathbf{u}^{\mathrm{T}},$$

where:

- $\mathbf{u} \in \mathbf{R}^3$ is a constant unit vector
- $[\mathbf{u}_\times] \in \mathbf{R}^{3\times 3}$ is the matrix of the cross-product by $\mathbf{u}$, namely

$$[\mathbf{u}_\times] = \begin{pmatrix} 0 & -\mathbf{u}_3 & \mathbf{u}_2 \\ \mathbf{u}_3 & 0 & -\mathbf{u}_1 \\ -\mathbf{u}_2 & \mathbf{u}_1 & 0 \end{pmatrix}.$$

- $\psi(t) \in \mathbf{R}$ is the angle of the rotation

The measurements can then be written as

$$a(t) = R(t)^{\mathrm{T}}\mathbf{a} = r_{\mathbf{u}}(-\psi(t))\mathbf{a}$$

If $a(t)$ is constant over time it does not provide any information about the rotation. This happens only in the two (nonexclusive) following cases:

- $\mathbf{u}$ and $\mathbf{a}$ are collinear, in which case $a(t) = \mathbf{a}$ for all t
- ψ is constant over time, in which case $a(t) = r_{\mathbf{u}}(-\psi)\,\mathbf{a}$ for all t

Apart from these cases, in the following we assume that $\mathbf{a}$ and $\mathbf{u}$ are linearly independent and that ψ varies.

15.2.1 Estimation Principle

The coordinates of $a(t)$ are a parametric representation of a curve contained in a plane orthogonal to $\mathbf{u}$, as shown in Figure 15.2, unambiguously defining the direction of $\mathbf{u}$. Without loss of generality, we consider that $\mathbf{u}$ is the vertical inertial vector $\mathbf{u} = (0\ 0\ 1)^{\mathrm{T}}$. We have

$$a(t) = \cos\psi(t)\,\mathbf{a} - \sin\psi(t)\begin{pmatrix}0\\0\\1\end{pmatrix}\times\mathbf{a} + (1-\cos\psi(t))\mathbf{a}_3\begin{pmatrix}0\\0\\1\end{pmatrix}$$

such that

$$a_1(t) = \cos\psi(t)\,\mathbf{a}_1 + \sin\psi(t)\,\mathbf{a}_2$$

$$a_2(t) = -\sin\psi(t)\,\mathbf{a}_1 + \cos\psi(t)\,\mathbf{a}_2$$

$$a_3(t) = \mathbf{a}_3.$$

Thus, all information about the angle is contained in the first two coordinates of the measurements. For convenience, we gather them into a single, complex-valued variable

$$y(t) \triangleq a_1(t) - ia_2(t) = \mathrm{e}^{i\psi}\left(\mathbf{a}_1 - i\mathbf{a}_2\right) \in \mathbf{C}, \tag{15.2}$$

where i is the usual unit imaginary number. The natural estimate $\hat{\psi}$ of ψ

$$\hat{\psi} = \arg_{-\pi} y,$$

where $\arg_{-\pi}$ (the argument determination in $[-\pi, \pi)$) determines ψ up to the argument of $\mathbf{a}_1 - i\mathbf{a}_2$, which is known by assumption.

In practice, the measurements are available at a sampling frequency $1/\Delta t$. A natural estimate of $\psi[k] = \psi\,(k\Delta t)$ is simply $\hat{\psi}[k] = \arg_{-\pi} y[k]$ or, to account for the cumulative angle (e.g., to count turns), and not only its value in $[-\pi, \pi)$

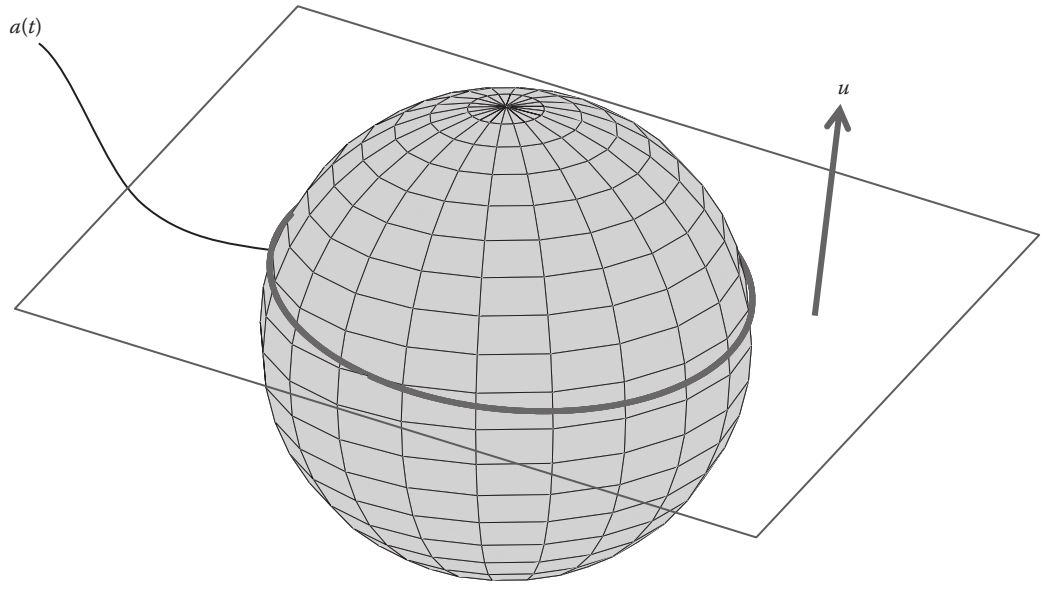

FIGURE 15.2 $a(t)$ describes a curve in a plane orthogonal to u.

$$\hat{\psi}[k] = \sum_{j=1}^{k-1} \arg_{-\pi} \frac{y[j+1]}{y[j]}. \tag{15.3}$$

15.2.2 Simulation Results

We illustrate the behavior of estimator (Equation 15.3) on simulations of the rotation of a satellite during a rest-to-rest reorientation maneuver, in which for $t \in [0,3]$, $\ddot{\psi}(t) = 1$, and for $t \in [3,6]$, $\ddot{\psi}(t) = -1$. We consider several sampling rates ranging from 10 to 100 Hz and signal-to-noise ratio ranging from 30 dB (noise over signal amplitude ≃22%) to 5 dB (noise over signal amplitude ≃78%). Typical results are pictured in Figure 15.3; numerical results are listed in Table 15.1. As expected, the estimation error increases with noise amplitude; however, the sampling rate does not seem to affect the error standard deviation.

It appears that the angle ψ is well estimated and that the spin motion of the satellite is relatively accurately estimated, enabling monitoring strategies. Post-filtering of the estimate can also be used online or offline (to avoid filtering lag) to smooth out visible artifacts. The estimation algorithm itself consists of simple arithmetical operations. No pre-filtering of data was employed.

15.2.3 Further Discussions

A detailed analysis of the estimation error $\hat{\psi}[k] - \psi[k]$ is presented in [6]. The impact of sampling frequency, measurement noise, and sensor discrepancies (e.g., biases, nonlinearities) is explicitly

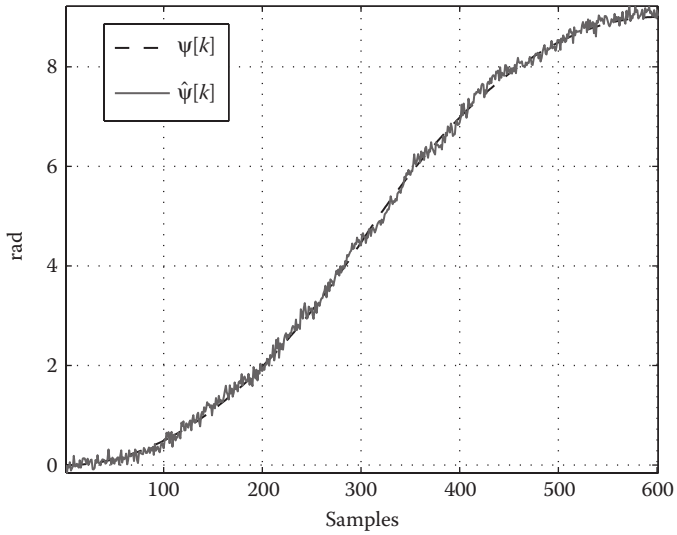

FIGURE 15.3 $\hat{\psi}[k]$ matches $\psi[k]$ from the start to the end of the maneuver (simulated results).

TABLE 15.1
Standard Deviation of Estimated Error for Various SNR and Sampling Rates

	ν_s = 100 Hz	ν_s = 50 Hz	ν_s = 10 Hz
SNR = 30 dB	σ = 5.7°	σ = 6.3°	σ = 6.5°
SNR = 13 dB	σ = 14.2°	σ = 13.5°	σ = 14.4°
SNR = 5 dB	σ = 24.5°	σ = 23.8°	σ = 22.9°

quantified. In particular, to account for sensor biases, it might be interesting to calculate the cumulative angle of the $y[j]$ samples with respect to a carefully chosen origin $z_0 \neq 0$. In such a case, estimator (Equation 15.3) is rewritten as

$$\hat{\psi}[k] = \sum_{j=1}^{k-1} \arg_{-\pi} \frac{y[j+1] - z_0}{y[j] - z_0}.$$

For application in practice, z_0 could be chosen as

- The mean of the measurements $y[j]$
- The Chebyshev center of the convex hull of the measurements $y[j]$

The latter choice is more robust for nonhomogeneously distributed data, but it induces computational burden.

15.3 DRIFTING AXIS

We now consider the more complex problem of small displacement of the rotation axis. This is still not a general case, since it does not account for every possible rotation; yet, the problem is of practical importance and cannot be fully reduced to a simple phase estimation as in Section 15.2.

We use the "ZXZ" Euler angle parametrization of the rotation matrix R as defined in [4]. These are recalled in Figure 15.4.

Again, we use the complex-valued variable $y \triangleq a_1 - ia_2$, which is a projection of the measurement a onto a horizontal plane. Using the Euler angle expression of the rotation matrix yields

$$\begin{aligned} y &= \mathbf{a}_1\left(\cos\varphi\cos\psi - \sin\varphi\sin\psi\cos\theta + i(\cos\varphi\sin\psi + \sin\varphi\cos\psi\cos\theta)\right) \\ &\quad + \mathbf{a}_2\left(\sin\varphi\cos\psi + \cos\varphi\sin\psi\cos\theta - i(-\sin\varphi\sin\psi + \cos\varphi\cos\psi\cos\theta)\right) \\ &\quad + \mathbf{a}_3(\sin\psi\sin\theta - i\cos\psi\sin\theta) \\ &= \mathbf{a}_1\left(\cos(\varphi+\psi) + i\sin(\varphi+\psi) + (1-\cos\theta)(\sin\varphi\sin\psi - i\sin\varphi\cos\psi)\right) \\ &\quad + \mathbf{a}_2\left(\sin(\varphi+\psi) - i\cos(\varphi+\psi) - (1-\cos\theta)(\cos\varphi\sin\psi - i\cos\varphi\cos\psi)\right). \end{aligned}$$

In the end, the measurement can be written

$$y = \frac{\mathbf{a}_1 - i\mathbf{a}_2}{2}(1+\cos\theta)e^{i(\varphi+\psi)} - i\mathbf{a}_3\sin\theta e^{i\psi} + \frac{\mathbf{a}_1 + i\mathbf{a}_2}{2}(1-\cos\theta)e^{i(\psi-\varphi)}. \tag{15.4}$$

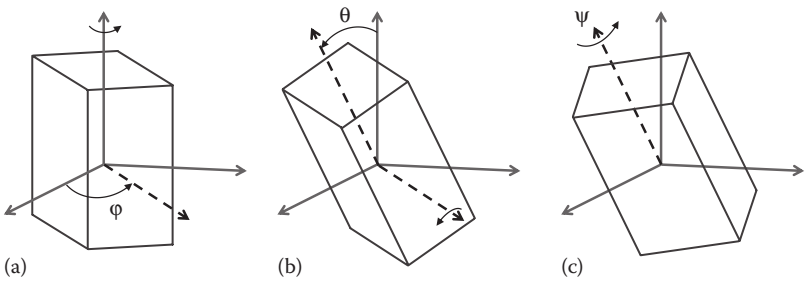

FIGURE 15.4 "*ZXZ*"–Euler angles. (a) Precession, (b) nutation, and (c) spin.

Note that for $\theta = \varphi = 0$ this formula reduces to

$$y = (\mathbf{a}_1 - i\mathbf{a}_2)e^{i\psi},$$

which is exactly Equation 15.2. Mathematically, we can now formulate an estimation problem as follows.

Problem 15.1

From measurements of the form (Equation 15.4) where φ, ψ, θ are the respective precession, spin, and nutation angles of a rigid body, find estimates $\hat{\varphi}, \hat{\psi}, \hat{\theta}$ of the Euler angles φ, θ, ψ.

Remark 15.1
We have several choices when defining the inertial frame of reference, depending on the analysis we wish to perform. For example, we may exhibit the nonobservability of the rotation angle around the reference vector $\mathbf{a}$ *as follows. If the inertial frame is chosen such that* $\mathbf{a}_1 = \mathbf{a}_2 = 0$, $\mathbf{a}_3 = 1$, *the measurement equation (15.4) reduces to* $y = -i \sin\theta e^{i\psi}$. *In this form, it is clear that angles* ψ *and* θ *are observable and that* φ *is not, as it does not affect the measurement. Thus, Problem 15.1 does not have a satisfactory solution in the general case. Typically, troubles arise if the rigid body precesses around the reference vector.*

In this section, we consider the example of a ballistic launch where the rotation axis is slowly moving in a plane while the rigid body has a high-spin angular rate. A typical example is a high-spin projectile traveling in ballistic mode after a shot (or, for an everyday object, a spinning football as represented in Figure 15.5).

Typical measurements $a(t)$ on the unit sphere and their projection onto a horizontal plane are shown in Figure 15.6.

15.3.1 Estimation Principle

For the motion under consideration, we formulate the following assumption.

Assumption 15.1
The precession φ is negligible compared to the spin ψ.
Under this assumption, we rewrite an approximated version of Equation 15.4 with $\varphi = 0$, which yields

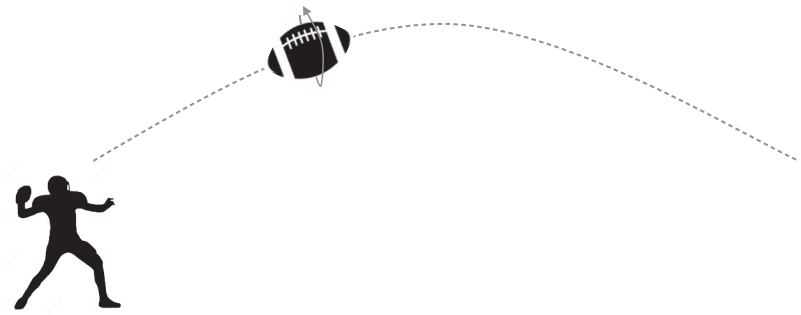

FIGURE 15.5 Typical example of a drifting axis motion.

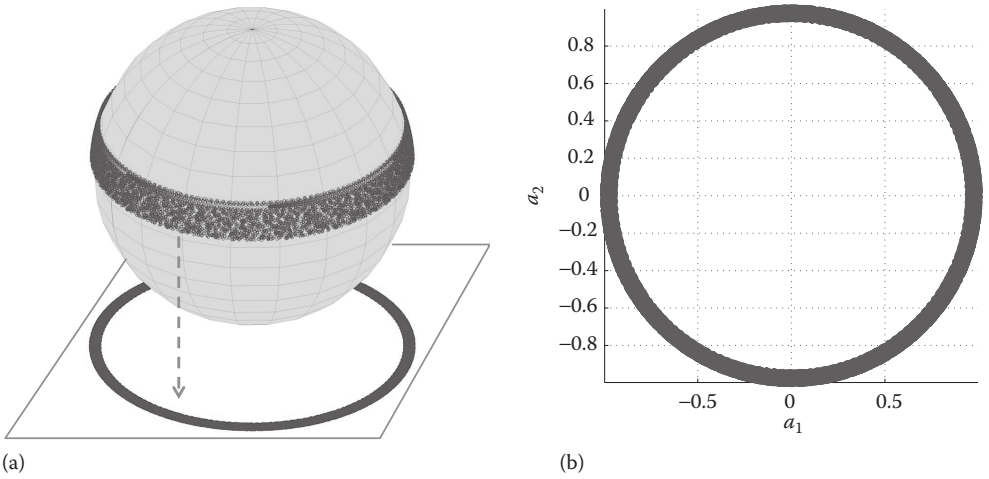

FIGURE 15.6 (Left) $a(t)$ draws circles slowly moving up the unit sphere. (Right) Projection onto a horizontal plane.

$$\begin{aligned} y &\simeq \left(\mathbf{a}_1 - i\mathbf{a}_2\cos\theta + i\mathbf{a}_3\sin\theta\right)e^{i\psi} \\ &= \sqrt{\mathbf{a}_1^2 + \left(\mathbf{a}_3\sin\theta - \mathbf{a}_2\cos\theta\right)^2}\, e^{i(\psi+\zeta(\theta))}, \end{aligned} \tag{15.5}$$

where $\zeta(\theta) \triangleq \arg_{-\pi}(\mathbf{a}_1 - i\mathbf{a}_2\cos\theta + i\mathbf{a}_3\sin\theta)$ is a known function of θ. The quantity $\psi + \zeta(\theta)$ is given from y by the estimator (Equation 15.3). The modulus of y is

$$|y| = \sqrt{\mathbf{a}_1^2 + \left(\mathbf{a}_3\sin\theta - \mathbf{a}_2\cos\theta\right)^2},$$

which allows us to find θ and, in turn, ψ. A schematic view of this simple algorithm is represented in Figure 15.7.

15.3.2 Simulation Results

This simple algorithm was tested on data for a projectile produced by the simulator FQW98 developed by V. Fleck at French–German Research Institute of Saint-Louis, France.* This high-fidelity simulator accounts for [3] gravity, wind, aerodynamic forces (drag, lift, Magnus effect) and torques, and the Coriolis effect.

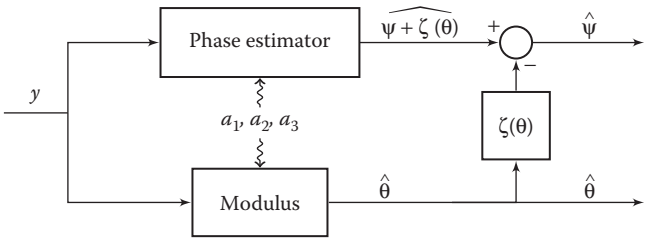

FIGURE 15.7 Estimation of ψ, θ for Assumption 15.1.

* We thank S. Changey from ISL for providing the dataset.

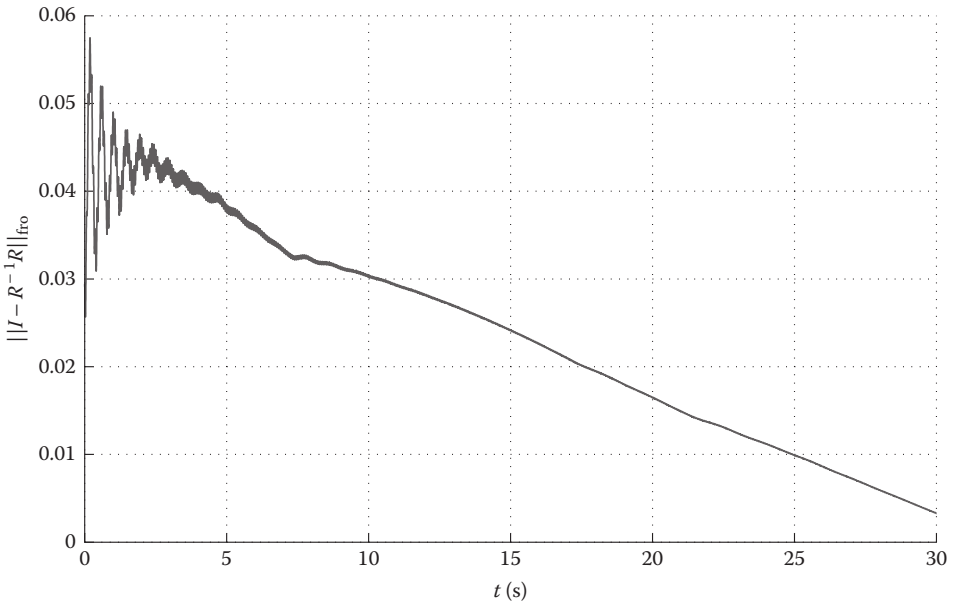

FIGURE 15.8 Estimation error in Frobenius norm (simulated results).

The parameters of this simulation are as described in [2]. The inertial frame is radial to the Earth's surface and defined by the launch site latitude and launch azimuth:

- Launch site latitude (45° north) and altitude 170 m
- Launch azimuth (1.5° east) and slope (25°)
- Initial linear velocity 684 m/s and angular rate $\omega = (0\ 0\ 78500)^{\mathrm{T}}$ °/s

The magnetic field measurements are those shown in Figure 15.6. The precession φ (not represented) remains less than 2.5°. The matrix $\hat{R}$ is computed from the estimated angles $\hat{\psi}, \hat{\theta}$, with $\hat{\varphi} = 0$. The norm of the estimation error $I - R^{-1}\hat{R}$ is reported in Figure 15.8.

15.4 TILTING AXIS

We now address Problem 15.1 for a second kind of motion in which the rotation axis is tilting. This is typically the case of long-axis mode celestial bodies such as the asteroid 4179 Toutatis [8] or, for an everyday object, the spinning top shown in Figure 15.9. It is also observed on smaller objects such as space debris [1]. Such motions are characterized by a small nutation, and Assumption 15.1 is then replaced by Assumption 15.2.

Assumption 15.2

The nutation θ is small and satisfies

$$\sqrt{\mathbf{a}_1^2 + \mathbf{a}_2^2}\ \theta \ll |\mathbf{a}_3|.$$

In the following, we invoke arguments of frequency separation in signal processing to explain how the sought-after information on the angles can be obtained from the measurements, with careful assumptions.

FIGURE 15.9 Typical tilting-axis motion.

15.4.1 Frequency Analysis of the Measurement Equation

We rewrite the measurement equation (15.4) as

$$y(t) = y_1(t)e^{i\phi_1(t)} + y_2(t)e^{i\phi_2(t)} + y_3(t)e^{i\phi_3(t)}, \tag{15.6}$$

with

$$\begin{aligned} \phi_1 &\triangleq \varphi + \psi \qquad & y_1 &\triangleq (\mathbf{a}_1 - i\mathbf{a}_2)\frac{1+\cos\theta}{2} \\ \phi_2 &\triangleq \psi & y_2 &\triangleq i\mathbf{a}_3 \sin\theta \\ \phi_3 &\triangleq \psi - \varphi & y_3 &\triangleq (\mathbf{a}_1 + i\mathbf{a}_2)\frac{1-\cos\theta}{2}. \end{aligned}$$

In this form, the measurement is the sum of three terms containing phase ϕ_i and modulated amplitude y_i. Interestingly, if ϕ_i, y_i and their derivatives satisfy some desired properties, we can recover the instantaneous frequencies $d\phi_i/dt$ using windowed Fourier transforms (see Chapter 4.4 in [5]) as explained below, giving a solution to the source separation problem.

According to Assumption 15.2, we have

$$\begin{aligned} y_1 &= (\mathbf{a}_1 - i\mathbf{a}_2)\left(1 + \mathcal{O}(\theta^2)\right) \\ y_2 &= i\mathbf{a}_3\theta\left(1 + \mathcal{O}(\theta^2)\right) \\ y_3 &= (\mathbf{a}_1 + i\mathbf{a}_2)\theta^2\left(\frac{1}{4} + \mathcal{O}(\theta^2)\right), \end{aligned}$$

which implies $|y_3| \ll |y_1|, |y_2|$. Thus, we consider an approximation of the measurements (Equation 15.6) of the form

$$y = y_1(t)e^{i\phi_1(t)} + y_2(t)e^{i\phi_2(t)}. \tag{15.7}$$

Although we appear to lose generality, it should be noted that the following analysis could (with additional tedious but relatively easy calculations) be extended to the general case (Equation 15.6). Practical implementation remains simple.

Let g be a (window) function even, positive, with finite support in $[-(1/2),(1/2)]$ and unit L_2 norm

$$\int_{-1/2}^{1/2} g^2(t)dt = 1.$$

Its Fourier transform $\mathcal{G}$ defined by

$$\mathcal{G}(\nu) = \int_{-\infty}^{\infty} g(t)\mathrm{e}^{-i\nu t}dt$$

satisfies

$$\mathcal{G}(0) \geq \mathcal{G}(\nu), \quad \forall \nu$$

and decays rapidly to 0 as ν increases. This decay is characterized by (among others) the bandwidth $\Delta\nu$ defined as

$$\left|\mathcal{G}\left(\frac{\Delta\nu}{2}\right)\right| = \frac{|\mathcal{G}(0)|}{\sqrt{2}}$$

In general, we have

$$\mathcal{G}(\nu) \ll \mathcal{G}(0), \quad \forall |\nu| \geq 2\Delta\nu$$

Take a scaling factor $s > 0$ and define the windowed Fourier transform Sy (aka spectrogram [5]) of the signal y at time u and frequency v using g as window, scaled by s as

$$\begin{aligned} Sy(u,\nu) &= \frac{1}{s}\int_{-s/2}^{s/2} y(u+t)\,g\left(\frac{t}{s}\right)\mathrm{e}^{-i(u+t)\nu}dt \\ &= \frac{1}{s}\int_{-s/2}^{s/2} y_1(u+t)\,g\left(\frac{t}{s}\right)\mathrm{e}^{i[\phi_1(u+t)-(u+t)\nu]}dt \\ &\quad + \frac{1}{s}\int_{-s/2}^{s/2} y_2(u+t)\,g\left(\frac{t}{s}\right)\mathrm{e}^{i[\phi_2(u+t)-(u+t)\nu]}dt \\ &\triangleq S_1(u,\nu) + S_2(u,\nu) \end{aligned}$$

The spectrogram satisfies the following property (for a proof, see Theorem 4.5 in [5]):

$$S_j(u,\nu) = y_j(u)\mathrm{e}^{i(\phi_j(u)-\nu u)}\mathcal{G}\left(s(\nu-\dot{\phi}_j(u))\right) + \varepsilon_j(u,\nu)\cdot$$

with

$$|\varepsilon_j(u,\nu)| \leq \frac{s}{2\sqrt{3}}|\dot{y}_j(u)| + \frac{s^2}{8\sqrt{5}}|\ddot{y}_j|_u + |y_j(u)|\frac{s^2}{8\sqrt{5}}|\ddot{\phi}_j|_u, \tag{15.8}$$

where $|\cdot|_u$ designates the supremum over $[u - s/2, u + s/2]$.

Assuming the error terms ε_j are small, the spectrogram reduces to two main terms

$$Sy(u,\nu) \simeq y_1(u)\mathrm{e}^{i(\phi_1(u)-\nu u)}\mathcal{G}\left(s(\nu-\dot{\phi}_1(u))\right) + y_2(u)\mathrm{e}^{i(\phi_2(u)-\nu u)}\mathcal{G}\left(s(\nu-\dot{\phi}_2(u))\right).$$

Thus, if the instantaneous frequencies $\dot{\phi}_1$ and $\dot{\phi}_2$ are sufficiently separated with respect to the bandwidth of $\mathcal{G}$, that is, if they satisfy

$$s\left|\dot{\phi}_1 - \dot{\phi}_2\right| \geq 2\Delta\nu \tag{15.9}$$

then $|S(u, \cdot)|$ has two main lobes for

$$\nu_j \triangleq \dot{\phi}_j(u),\ j = 1,2.$$

More precisely, we have

$$Sy(u, \dot{\phi}_j(u)) \simeq y_j(u) e^{i[\phi_j(u) - u\dot{\phi}_j(u)]} \mathcal{G}(0).$$

Hence, we can recover the instantaneous frequencies $\dot{\phi}_j(u)$ by detecting the peaks of the spectrogram [5]. Further, the corresponding amplitude of the lobe gives us $y_j(u)$. These items of information allow us to estimate the three Euler angles.

If separating condition (Equation 15.9) is met, the decay of $\mathcal{G}$ suffices to isolate the contributions of $S_1(u, \dot{\phi}_1(u))$ and $S_2(u, \dot{\phi}_2(u))$ in the frequency domain. To safely consider that detection of the spectrogram peaks will give a satisfactory result, we need to verify that none of the six terms of Equation 15.8 for $j = 1,2$ disturbs the location of any of the peaks $\nu = \dot{\phi}_1(u), \dot{\phi}_2(u)$. Considering Equation 15.8 together with the fact that the peak at frequency $\nu = \dot{\phi}_j(u)$ has amplitude

$$|\, y_j(u)\, |\, \mathcal{G}(0)$$

allows us to derive the following set of conditions that, along with the separating condition (Equation 15.9), guarantees the reliability of detecting the peaks:

$$s\left|\dot{y}_j\right| \ll 2C_1\left|y_j\right|, \tag{15.10}$$

$$s^2\left|\ddot{y}_j\right|_u \ll C_2\left|y_j(u)\right|, \quad \forall u \tag{15.11}$$

$$s^2\left|\ddot{\phi}_j\right| \ll C_2, \tag{15.12}$$

where we have denoted

$$C_1 \triangleq 2\sqrt{3}\mathcal{G}(0), \quad C_2 \triangleq 8\sqrt{5}\mathcal{G}(0).$$

When g is for instance a normalized Hann window [5], we have

$$\Delta\nu \simeq 9.05 \text{ rad}, \quad C_1 \simeq 2.83, \qquad C_2 \simeq 14.61$$

If conditions (15.10 through 15.12) hold, a study of the arguments and values of the local maxima of Sy will then give a convenient and reliable solution to the stated problem. In detail, we use the following algorithm, represented in Figure 15.10 for convenience.

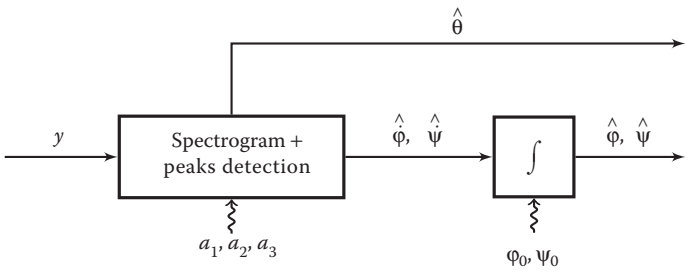

FIGURE 15.10 Estimation of φ, θ, ψ under Assumption 15.2 and conditions (15.9 through 15.12).

Algorithm 15.1

Solution to Problem 15.1 under Assumption 15.2 and conditions (15.9 through 15.12)
Inputs:

- Sampled data $y[k]$, sampling time $t[k]$
- Window function g
- Window size s

Steps for each $t[k]$:

- Calculate the spectrogram $Sy(t[k], \cdot)$ (e.g., by mean of a fast Fourier transform)
- Find the two main lobes of $|Sy(t[k], \cdot)|$ corresponding to frequencies v_1, v_2 with $|v_1| > |v_2|$ and amplitudes A_1, A_2 (e.g., by an exhaustive search of local maxima)
- Compute estimates

$$\widehat{\frac{d\varphi}{dt}}[k] = \nu_1 - \nu_2, \quad \widehat{\frac{d\psi}{dt}}[k] = \nu_2$$

- Estimate $\varphi[k]$, $\psi[k]$ by cumulative numerical integration of the estimates of their respective derivative defined above
- Estimate $\theta[k]$ from

$$\widehat{\cos\theta}[k] = \frac{2A_1}{\sqrt{\mathbf{a}_1^2 + \mathbf{a}_2^2}\,\mathcal{G}(0)} - 1, \quad \widehat{\sin\theta}[k] = \frac{A_2}{|\mathbf{a}_3|\,\mathcal{G}(0)}.$$

Remark 15.2

- *The algorithm provides average values (over a time window of size s) of* $\dot{\varphi}$, $\dot{\psi}$, *and* θ. *Thus, it does not allow high-frequency variations (compared to 1/s) of these quantities to be observed*
- *The algorithm needs initial values of* φ *and* ψ *to estimate the full rotation*
- *The computation of* $Sy(t[k], \cdot)$ *requires the values of y over* $[t[k]-s/2, t[k] + s/2]$. *Therefore, it introduces a short lag*
- *The estimation of* $\theta[k]$ *can be implemented only if* $|\boldsymbol{a}_3|$ *is known*

15.4.2 Simulation Results

In this section, we illustrate the sensitivity of the algorithm with respect to the time-window size s. We simulate a rigid body as a homogeneous parallelepiped with semi-axes 0.5, 0.75, 1 m and mass 200 kg. The reference vector is assumed to have a constant value $\mathbf{a} = 1/\sqrt{3}(1\,1\,1)^{\mathrm{T}}$.

The dynamics of R is given by

$$\dot{R} = R\left[\omega_{\times}\right] \tag{15.13}$$

$$J\dot{\omega} = J\omega \times \omega + \tau \tag{15.14}$$

where:
ω is the angular rate of the rigid body
J is the matrix of inertia
τ is the external torque

In this simulation we assume that the Euler equation 15.14 is driven by a damping torque

$$\tau = -0.02\omega$$

Equations 15.13 and 15.14 are solved using a Runge–Kutta 4 numerical scheme with fixed time step 0.01 s.* We use the following initial conditions:

$$\omega(0) = (101\ 0\ 630)^{\mathrm{T}}\ ^\circ/\mathrm{s}, \quad \varphi(0) = 0, \quad \psi(0) = \frac{\pi}{2}, \quad \theta(0) = \frac{\pi}{8}.$$

The corresponding measurements are represented in Figure 15.11 evolving on the unit sphere and projected onto a horizontal plane.

For the windowed Fourier transforms we use a *Hann window* [5]

$$g(t) = 2\sqrt{\frac{2}{3}}\cos^2 \pi t$$

The estimation error for $s = 5$ s and $s = 3.5$ s is shown in Figure 15.12.

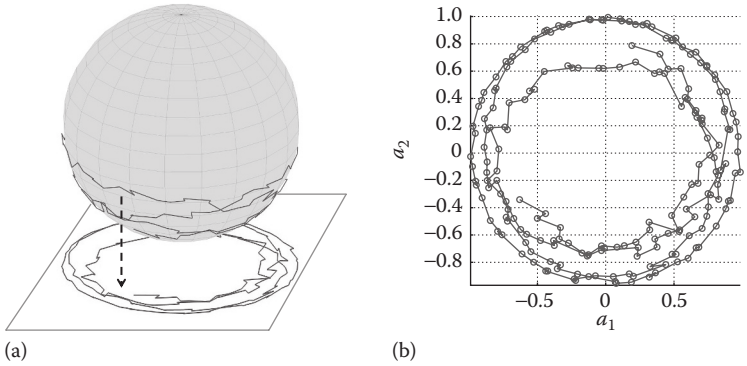

FIGURE 15.11 (a) Noisy measurements on the unit sphere; (b) projection onto a horizontal plane (simulated data).

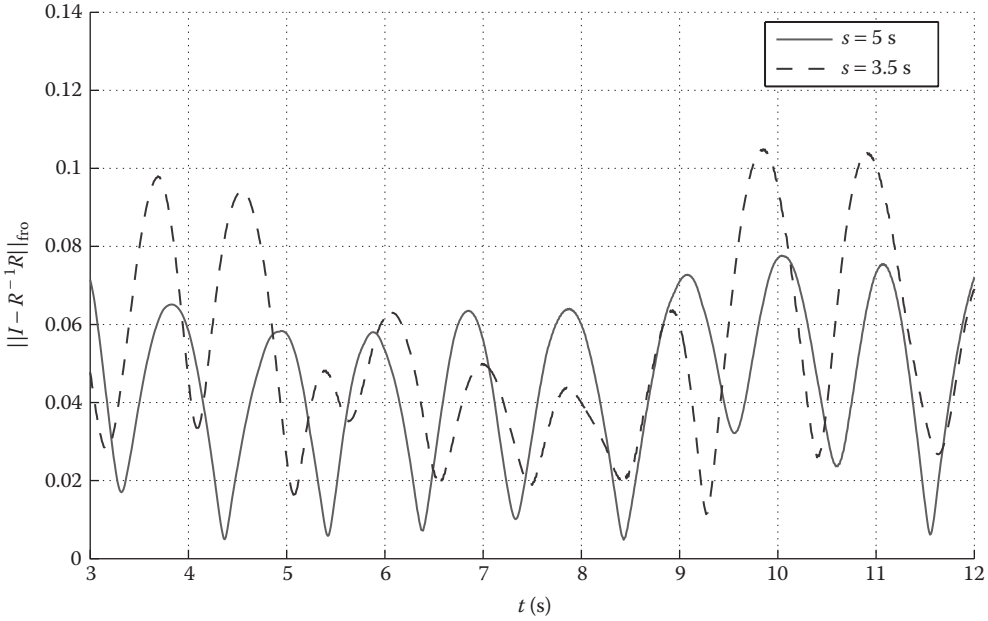

FIGURE 15.12 Estimation error in Frobenius norm (simulated results).

* For efficiency we compute a quaternion version of Equation 15.13.

Overall, the estimation is more precise for $s = 5$ s. Yet, on a small time interval, the smaller tuning $s = 3.5$ s shows better performance. This is not surprising when conditions (15.10 through 15.12) are considered, where small values of s are desirable, but too small a value of s may violate the frequency separation condition (15.9). To illustrate this point, we compute the corresponding spectrograms $|Sy|$ in Figure 15.13 for $s = 5$ s and $s = 3.5$ s. In both figures, we clearly see the two main lobes of the spectrogram and the peaks corresponding to frequencies ψ and $\varphi + \psi$.

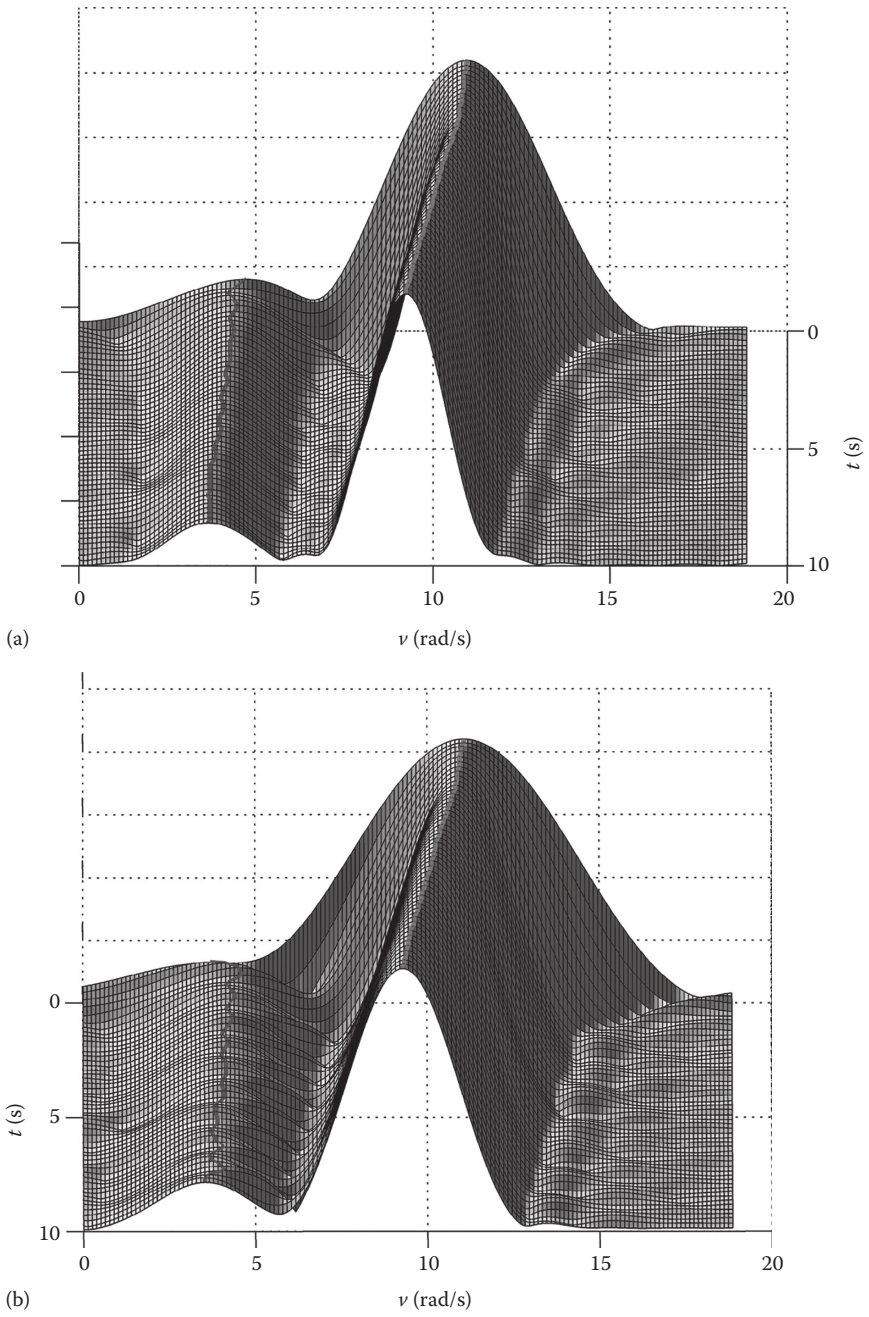

FIGURE 15.13 Spectrogram for $s = 5$ s (a) and $s = 3.5$ s (b).

For $s = 3.5$ s, the peaks corresponding to ψ are corrupted by side oscillations of the main lobe. The estimation may become less accurate.

15.4.3 Further Discussions

Reference [7] presents a set of conditions equivalent to Equations 15.9 through 15.12 in the case of free-rotational motion. The equivalent conditions bear on the principal moments of inertia of the rigid body and two initial values only: the angular momentum and the initial nutation.

15.5 CONCLUDING REMARKS

In this chapter, we have exposed three cases of rotational motions of increasing complexity which can be estimated from single vector measurements. Some assumptions guaranteeing the nonambiguity of the measurements have been established.

The resulting estimators are straightforward, easy to implement, and induce low computational burden.

The problems in the study are relatively general. Specific studies could be conducted in a similar manner for other governing dynamics: the aerodynamics of atmospheric flight could be considered explicitly.

BIBLIOGRAPHY

1. C. Bonnal, J.-M. Ruault, and M.-C. Desjean. Active debris removal: Recent progress and current trends, *Acta Astronautica*, 85, 51–60, 2013.
2. S. Changey. Modélisation et estimation par filtrage non linéaire, de l'attitude d'un projectile à partir de magnétomètres. PhD thesis, French-German Research Institute, Saint-Louis, France, 2005.
3. V. Fleck. *Introduction à la Balitistique Extérieure*. Coetquidan, France: ISL, 1998.
4. L. Landau and E. Lifchitz. *Mechanics*. Moscow, Russia: MIR, 1982.
5. S. Mallat. *A Wavelet Tour of Signal Processing*. San Diego, CA: Academic Press, 1998.
6. L. Magnis and N. Petit. Rotation estimation for a satellite from Sun sensors. In *European Control Conference*, IEEE, Zurich, Switzerland, pp. 852–859, 2013.
7. L. Magnis and N. Petit. Estimation of 3D rotation for a satellite from Sun sensors. In *Proceedings of the 19th IFAC World Congress*. IFAC, Cape Town, South Africa, pp. 10004–10011, 2014.
8. B. E. Mueller, N. H. Samarasinha, and M. J. Belton. The diagnosis of complex rotation in the lightcurve of 4179 Toutatis and potential applications to other asteroids and bare cometary nuclei, *Icarus*, 158(2), 305–311, 2002.